FACULTY OF INFORMATION TECHNOLOGY AND ELECTRICAL ENGINEERING
DEGREE PROGRAMME IN WIRELESS COMMUNICATIONS ENGINEERING

MASTER'S THESIS

UTILIZING VECTOR NETWORK ANALYZER FOR MEASURING COMPLEX DIELECTRIC CONSTANT OF INDOOR WALLS

Author	Fahmida Afroz Lopa
Supervisor	Risto Vuohtoniemi
Second Examiner	Markus Berg
(Technical Advisor	Veikko Hovinen)

March 2020

Lopa F. (2020) Utilizing vector network analyzer for measuring complex dielectric constant of indoor walls. The University of Oulu, Faculty of Information Technology and Electrical Engineering, Degree Programme in Wireless Communications Engineering. Master's Thesis, 46 p.

ABSTRACT

In this thesis, a two-port vector network analyzer (VNA) and double-ridged waveguide horn antennas (Rohde & Schwarz HF906) were utilized for assessing the complex relative permittivities of building materials. The measurements were done in two different frequency bands in the University main building in Linnanmaa, Oulu. Reflection coefficients of different walls were measured in the lecture room PR102. The measurement data were collected at lower frequency range of 1-9.5 GHz and at upper frequency range of 9.5-18 GHz.

An absorbing non-conductive material has a complex valued permittivity, whose quality can be assessed by fitting the theoretical reflection coefficient curve on the measured values over a large range of angles of incidence at parallel polarization. The reflection coefficients were estimated from the measured data taking into account the increased attenuation due a longer path length. After applying the path length compensation, coefficients falling within one degree from each other are averaged to give the data equal weighing over the abscissa. The dielectric constants were assessed for a brick wall with a smooth surface and a wall with a rougher surface. The value of complex dielectric constant in range of (3.7-4.22)-j(0.73-0.03) was found to be in accordance with results published by the International Telecommunications Union.

The measurement system was able to perform efficiently for the proposed objective of the study. Several improvements can be made in future to adopt a more accurate measurement system to study the reflection characteristics of building materials. The aim of this thesis is to effectively use a vector network analyzer for measuring material properties by inspecting the reflection of a parallel polarized electromagnetic wave from a flat surface of material samples.

Keywords: angle of incidence, reflection coefficient of indoor brick wall, root mean square error, Brewster's angle, complex permittivity, dielectric constant, vector network analyzer (VNA).

TABLE OF CONTENTS

FOREWORD

The thesis work is completed at Centre for Wireless Communications research unit at the University of Oulu as partial fulfilment of the master's degree requirements in Wireless Communications Engineering. I am very much grateful to Centre for Wireless Communications as well as the University of Oulu, which established for an academic platform and learning environment to think and grab actual things behind the scene as out of the box that enhances my skillset.

I would like to give special thanks to my technical advisor M.Sc. (Tech.) Veikko Hovinen for his direct nonstop support throughout the entire period of my master's thesis journey. Your guidance at each stage made the timely accomplishment of the work possible. I would also thank you sincerely to my supervisor Lic.Sc (Tech) Risto Vuohtoniemi and Docent Markus Berg for their great ideas leading to this work. Both of your support, comments, and reviews were crucial for the completion of the thesis.

Love to my family members for their love and support that I have enjoyed during my University studies. Special thanks go to my husband, Md Chapal Shaik, for the sincere support and understanding of my passion for science for all the years we have been together. I also would like to thank my daughter, who joined us when I was writing my dissertation for giving me unlimited happiness and pleasure. My dedication is to my parents and brother for their unconditional love, encouragement, and support. Finally, I am also grateful to the Finnish education authority to provide me with the opportunity to pursue my master's degree.

Oulu, Finland, March 31, 2020

Fahmida Afroz Lopa

LIST OF ABBREVIATIONS AND SYMBOLS

3D	Three dimensional
DC	Direct current
GRP	Glass-reinforced plastic
GPIB	General purpose interface bus
LOS	Line-of-sight
PSO	Particle swarm optimization
RC	Reflection coefficient
RF	Radio frequency
RT	Ray-tracing
RX	Receiver
RMSE	Root mean square error
SNA	Scalar network analyser
TDR	Time domain reflectometer
TFT	Thin film transistor
TX	Transmitter
VNA	Vector network analyzer

C	Constant for system losses
D	Dumping coefficient
$\boldsymbol{D}$	Electric flux density
$\boldsymbol{D_o}$	Electric flux density in free space
d	Link length, Distance
d_0	3D-distance between the transmitter and the receiver
d_1	3D-distance from the transmitter to the interaction point
d_2	3D-distance from the interaction point to the receiver
d_{LOS}	LOS path length
$\boldsymbol{dp_i}$	Orientational polarization dipole
$\boldsymbol{E}$	Electric field
E_1	Incident field strength in medium 1
$E_{1,\parallel}$	Incident field strength of p-polarization in medium 1
$E_{1,\perp}$	Incident field strength of s-polarization in medium 1
E'_1	Reflection field strength in medium 1
$E'_{1,\parallel}$	Reflection field strength of p-polarization in medium 1
$E'_{1,\perp}$	Reflection field strength of s-polarization in medium 1
$\boldsymbol{E_a}$	Applied electric field
$E_r(\Theta)$	Receiver antenna pattern
E_x	Amplitude of x-component of the electric field
E_y	Amplitude of y-component of the electric field
G_r	Receiver antenna gain
G_t	Transmitter antenna gain
$\boldsymbol{H}$	Magnetic field
h	Channel response
K	Wave number
L	Path loss
L_{TX}	Transmitter losses

L_{FS}	Free space path loss
L_M	Miscellaneous losses
L_{RX}	Receiver losses
l_0	Steady-state solution at $t = 0$
$\boldsymbol{l_i}$	Distance between positive and negative dipole charges
l_p	Steady-state solution
M	Mass of the electrons
N	Number of multipath components, Path loss exponent, Number of sample values
N_e	Number of electric dipoles per unit volume
n	Path loss exponent
n_1	Refractive index of medium 1
n_2	Refractive index of medium 2
$\boldsymbol{P}$	Macroscopic steady-state electric polarization
P_{db}	Reflected power in dB scale
P_{LOS}	Power of line-of-sight path
P_r	Received power in linear scale
P_{REFL}	Power of reflected path in linear scale
P_t	Transmitted power in linear scale
$\boldsymbol{P_t}$	Total dipole moment of a material
RF	Radio frequency
Q	Dipole charge
q_{sp}	The bound surface of charge density
s_{11}	Input port reflection coefficient
s_{12}	Reverse gain
s_{21}	Transmission coefficient
s_{22}	Output port reflection coefficient
t	Time instant
$\hat{\mathbf{x}}$	Unity field vector in direction x
Y_i	Sample value
$\widehat{Y}_i$	Estimation value
$\hat{\mathbf{y}}$	Unity field vector in direction y

Δv	Volume
Θ_i	Angle-of-arrival of signal
Φ	Cross-polarized angle
α	Orientation angle,
α_i	Amplitudes of the multipath components
δ	Dirac delta function
ε	Complex permittivity
ε_0	Permittivity of free space
ε_1	Permittivity of medium 1
ε_2	Permittivity of medium 2
ε_r	Relative permittivity, Complex dielectric constant
ε_s	Static permittivity of the medium
ε'	Real part of the complex permittivity
ε''	Imaginary part of the complex permittivity
η	Wave impedance

θ	Diffraction angle
θ_i	Angle of incidence
θ_1	Angle of reflection
θ_B	Brewster's angle
θ_t	Angle of refraction
λ	Wavelength
ρ	Reflection coefficient
$\rho_\perp$	Reflection coefficient of s-polarization
$\rho_\parallel$	Reflection coefficient of p-polarization
τ_i	Time delay
φ_i	Phase shift
φ	Phase angle between x and y components

1. INTRODUCTION

In this era of communication, indoor wireless communications are among the fastest-growing sectors. Over the past decades, extensive development in radio communication systems has been witnessed. Growing demand for high performance and low-cost personal communication systems have made way for the development of indoor radio communication systems. A key to design an efficient wireless network, in-depth knowledge of radio wave propagation in the radio channel, is required. Radio channel characterization is the most important for system design and planning. Therefore, the building materials and their behaviour with the electromagnetic waves have to be characterized before designing an indoor propagation model [1].

Past decades, several researchers have studied ways to measure complex dielectric constant of various dielectric materials [1], [9], [8]. An observation into these results helps to utilize maximum efficient techniques for evaluation of the electromagnetic properties of building materials. In [1], a free space evaluation of reflection and transmission coefficients for measuring the complex dielectric constant of materials of building walls has been implemented. Frequency range from 2.4 to 17 GHz is measured using two orthogonal polarizations. A VNA was used for the measurement process with two horn antennas. The complex dielectric constant is assessed by using optimization. Two methods for calculating complex dielectric constant, namely the non-linear least square method and particle swarm optimization (PSO), were utilized. PSO was found to be a more efficient method as it yields smaller mean square error values. Parallel polarization shows a smaller value of complex dielectric constant compared to perpendicular polarization [1].

In this thesis, reflection coefficient of two walls were measured at 1-18 GHz frequency range using a vector network analyzer (VNA) and a pair of parallel polarized (p-polarized) horn antennas. The complex relative permittivity, i.e., the dielectric constant, was assessed by fitting the theoretical reflection curve on the normalized reflection measurement data. Root mean square error was used as a merit of fitting accuracy.

The measurements were conducted in a lecture hall on the Linnanmaa campus at the University of Oulu. The measurement targets were two different types of brick walls. Both of the walls were build using perforated bricks. The first wall has the bricks laid on side, producing a fairly smooth surface. The finish has been done with a layer of white paint. The second wall has the bricks laid on edge, so that the perforation is visible, producing a regular grid of open holes leading directly to a fiberglass insulation behind the wall. No finishing has been done on this wall. Both walls are several years old, and the moisture level is the one of the normal indoor air.

This thesis is organized as follows. In chapter 1, this thesis firstly gives the concept and aim of the whole work. Chapter 2 explains the background of electromagnetic wave propagation and radio channel characteristics. Chapter 3 explains the nature of polarization and its properties. Chapter 4 gives the idea of the reflection coefficient

and the complex dielectric constant and its effect. Chapter 5 elaborates about the measurement techniques. Chapter 6 presents the scenarios of the measurements and the analysis method, which established that the results are valid. Measurement results are introduced in Chapter 7. Chapter 8 discusses the results and possible improvements to the system. In chapter 9, the whole work is summarized. And finally, in the appendices, the immediate measurement results are shown as impulse response figures, followed by the curve fitting results.

2. RADIO CHANNEL CHARACTERISTICS

The radio channel is varying with time, environment, and other external factors. Radio channel has a significant impact on signal propagations. The electromagnetic energy propagates through different paths as shown in Figure 1. Transmitter produces an electromagnetic wave at a specific frequency. The transmission line feeds the radio frequency (RF) energy to the transmit antenna TX, and the radio propagation path passes the energy to the receiver. Before reaching the receiver antenna RX, the radio wave undergoes many physical phenomena caused by the radio channel, such as free-space loss, reflection, refraction, diffraction, and scattering.

In this thesis, the propagation phenomenon of interest is the reflection from the inspected flat surface, shown as a dashed rectangular in Figure 1. The reflected wave has a longer propagation path than the direct line-of-sight path d_{LOS} between TX and RX. This path difference can be easily calculated with the methods described in chapter 6. The reflected path of interest is denoted by sum distance $d_1 + d_2$, and drawn using thick blue line in Figure 1. All other reflections (green dotted lines) are not of interest, and can be neglected.

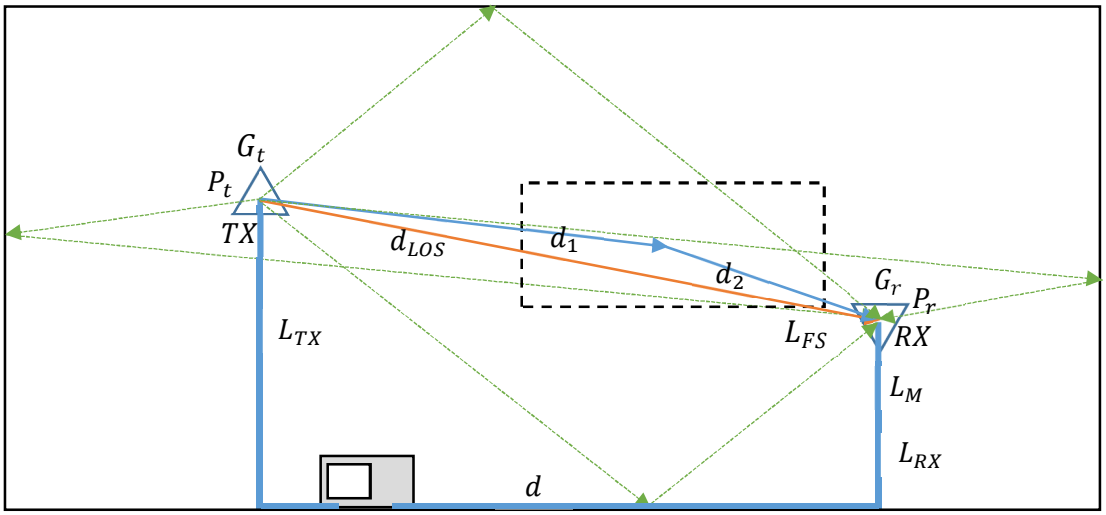

Figure 1. Concept of an indoor radio propagation measurement system and the reflected paths.

2.1. Free space propagation and path loss

For the propagation of radio signals, free space propagation is the simplest path loss model. Referring to the figure above, free space propagation of electromagnetic radiation is a straight-line path signal between the transmitter and the receiver with no atmospheric attenuation. Remote controllers, short-range indoor communication, and satellite links these are the example of free space propagation [4].

In general case when antenna separation d is much larger than the antenna heights, received power P_r can be calculated by [3]:

$$P_r = P_t G_t G_r \left(\frac{\lambda}{4\pi d}\right), \quad (1)$$

where G_t is transmitter antenna gain, G_r is receiver antenna gain, d is a distance of transmitter and receiver, λ is the wavelength of the signal, P_t is transmitted power, P_r is received power. P_t and P_r are in the same units in linear scale, and G_t and G_r are dimensionless quantities also in linear scale.

Path loss

Path loss describes the reduction of power per unit volume of an electromagnetic wave. The difference between the transmit power and the received power is called path loss.

Path loss is usually expressed in dB. Path loss can be calculated by using this formula [5]:

$$L = n10\ log_{10}(d) + C, \quad (2)$$

where L is path loss in decibels, n is path loss exponent, d is the distance between transmitter and receiver, and C is constant for system losses.

2.2. Multipath propagation

Multipath propagation is the phenomenon that happens when the radio signal takes two or more paths to the receiving antenna from the transmitting antenna.
In indoors, multiple signals from the transmit antenna reaching the receive antenna via either a direct line of sight, or by reflecting from objects such as walls, ceiling, floor, and furniture. These paths are shown as green dotted lines in Figure 1.

Linear filter $h(t)$ with a complex baseband impulse response is modelling multipath propagation at time instant t [11]:

$$h(t) = \sum_{i=1}^{N} \alpha_i e^{-j\varphi_i}\ \delta(t-\tau_i) E_r(\Theta_i)\ , \quad (3)$$

where α_i is amplitudes of the multipath components, φ_i is phase shifts, $\delta(t)$ is the Dirac delta function denoting an impulse at time instant t, τ_i is time delays, Θ_i is angle-of-arrival of signals, N is the number of multipath components, $E_r(\Theta)$ is receiving pattern.

2.3. Link budget

In transmission system, link budget is required for calculating all the gains and losses from the transmitter to the receiver. Using quantities shown in Figure 1, a simple link budget equation in decibel scale is given by [6]:

$$P_r = P_t + G_t - L_{TX} - L_{FS} - L_M + G_r - L_{RX}\,, \tag{4}$$

where P_r is receiver power, P_t is transmitter output power, G_t is transmitter antenna gain, L_{TX} contains the transmitter losses, L_{FS} is the free-space loss, L_M is miscellaneous losses, G_r is receiver antenna gain and L_{RX} contains the receiver losses.

2.4. Interaction with flat surface

When waves pass from one medium to another, interactions happen. There are three types of interaction of surface-based on straight light propagation [7]:

1. Radio wave reflection.
2. Radio wave refraction.
3. Radio wave diffraction.

The two phenomena based on wave propagation are reflection and refraction. The phenomenon of radio waves bouncing from an obstacle is called reflection. Radio wave reflection involves a change in the direction of waves when they bounce off a barrier. A mirror is an example of reflection [7].

Radio wave refraction involves a change in the direction of waves as they pass from one medium to another, as depicted in Figure 2.

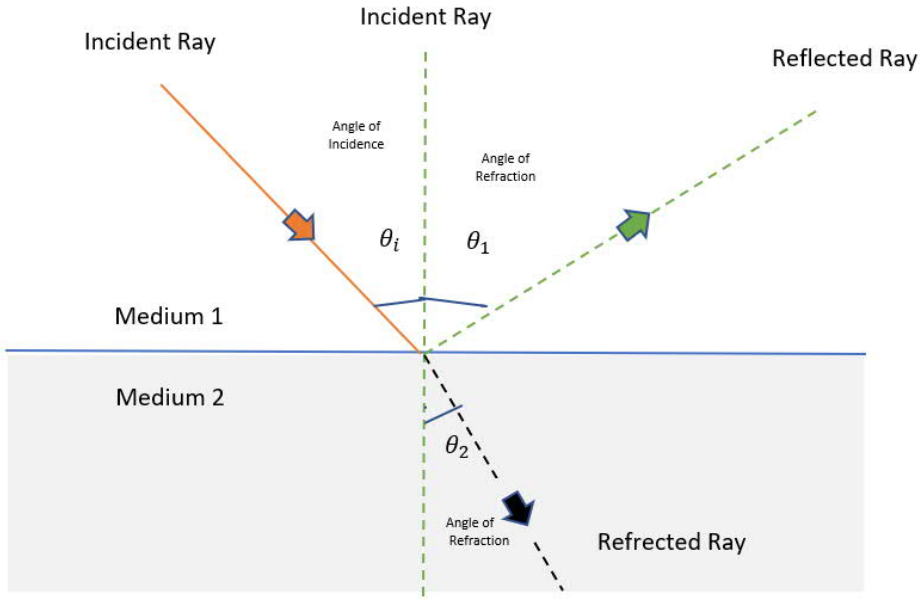

Figure 2. Radio wave reflection and refraction.

3. POLARIZATION

The polarization of the wave defines the alignment of the electric field vector $\boldsymbol{E}$ of a plane wave relative to the direction of propagation. Wave $\boldsymbol{E}$ propagating in the positive z-direction consists of two orthogonally polarized components **x** and **y**. The general expression for such a wave is [12]

$$\boldsymbol{E} = \left(\hat{\mathbf{x}}E_x + \hat{\mathbf{y}}E_y e^{j\varphi}\right)e^{-jkz} \ , \tag{5}$$

where E_x and E_y are real-valued scaling factors of orthogonal unity field vectors $\hat{\mathbf{x}}$ and $\hat{\mathbf{y}}$, φ is the phase angle between **x** and **y** components, e^{-jkz} is the exponential propagation factor for phasor wave, and $k = 2\pi/\lambda$ is the wave number. The corresponding magnetic field is

$$\boldsymbol{H} = \frac{1}{\eta}\left(-\hat{\mathbf{x}}E_y e^{j\varphi} + \hat{\mathbf{y}}E_x\right)e^{-jkz} \ . \tag{6}$$

Depending on the phase and the relative amplitudes E_x and E_y, there are three types of polarizations [13]:

1. Linear polarization.
2. Circular polarization.
3. Elliptical polarization.

The linear polarization is shown in Figure 3 [13]. The linear polarization at 45° can also be viewed as the addition of a horizontally linearly polarized wave and a vertically polarized wave of the same amplitude in the same phase.

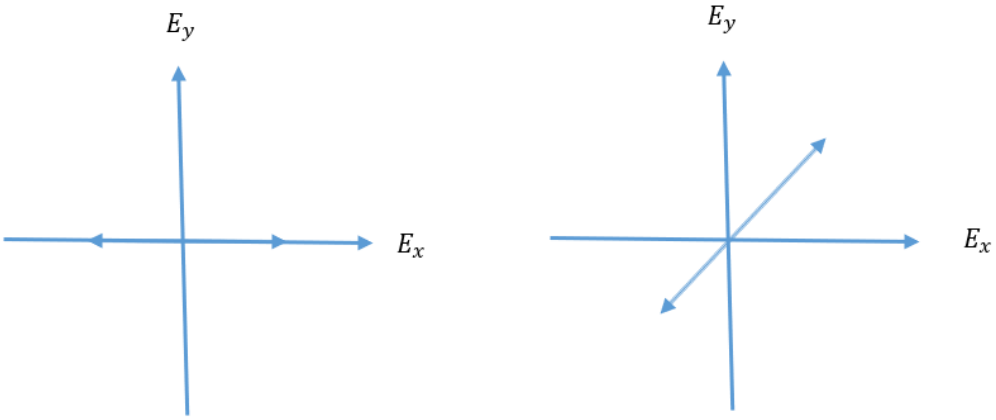

Figure 3. Linear polarization.

The circular polarization is shown in Figure 4 [13]. The electric field of circularly polarized wave consists of two perpendicular, equiamplitude, linear components that have a phase difference of π/2.

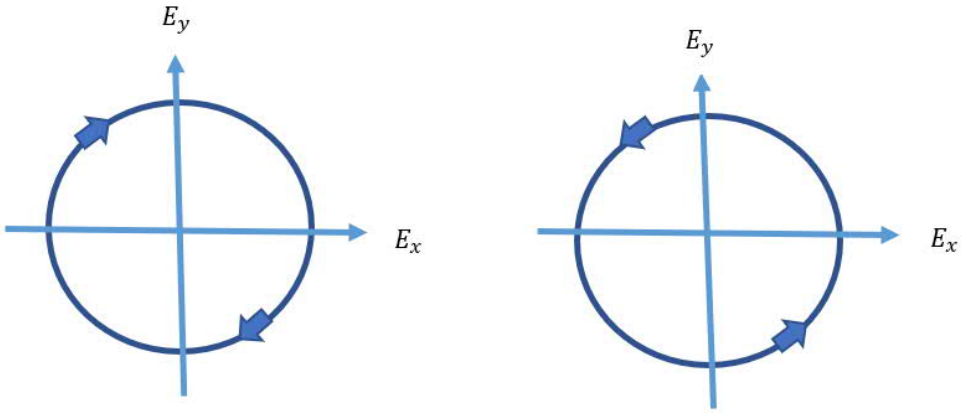

Figure 4. Circular polarization.

The elliptical polarization is shown in Figure 5 [13]. The electric field of elliptically polarized wave consists of two perpendicular linear components with any amplitude and phase differences.

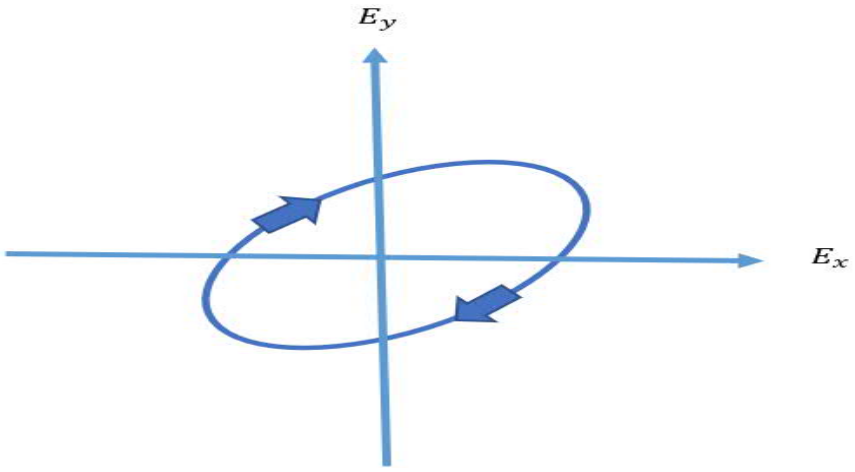

Figure 5. Elliptical polarization.

3.1. Linear polarization

When the two components are in phase, φ=0, the electric field vector defines a plane as its propagation in the z-direction by orientation angle α with respect to the x-axis, as illustrated in Figure 6 [12]:

$$\alpha = \tan^{-1}\left(\frac{E_y}{E_x}\right) . \tag{7}$$

For a linearly polarized wave, this angle α is the same for all values of z and t.

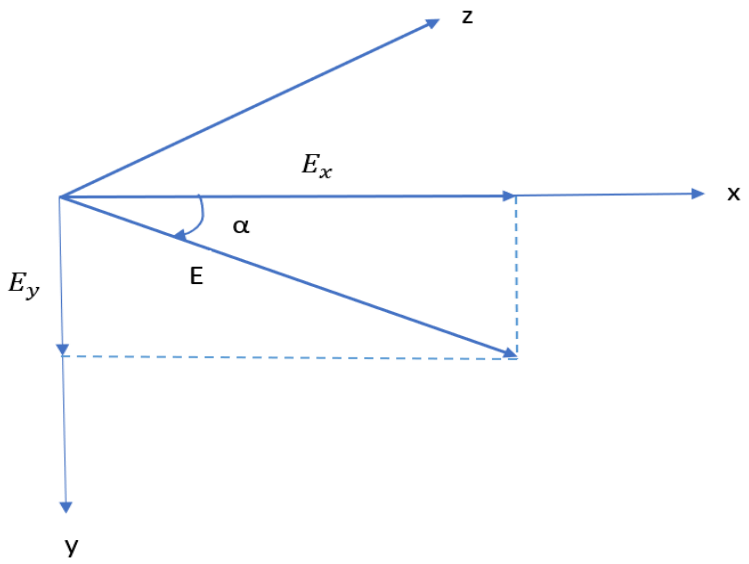

Figure 6. Linearly polarized wave.

3.2. Circular polarization

The circularly polarized field consists of two perpendicular electromagnetic planes (vertical or horizontal) waves of equal amplitude and the difference in phase by 90° [13]. A circularly polarized wave can rotate in two senses: $\varphi = -\frac{\pi}{2}$ is called the right-hand or clockwise and $\varphi = +\frac{\pi}{2}$ is also called the left-hand or counter-clockwise.

When amplitudes E_x and E_y are equal, and the phase angle is $\varphi = \pm\frac{\pi}{2}$, equation (5) then becomes [12]:

$$E = (\hat{x} \pm j\hat{y})E_x e^{-jkz}. \tag{8}$$

The corresponding magnetic field is [12]:

$$H = \frac{E_x}{\eta}(\pm j\hat{x} + \hat{y})e^{-jkz}. \tag{9}$$

3.3. Elliptical polarization

Elliptically polarized light consists of two perpendicular waves of unequal amplitude, which differ in phase by 90°. An elliptically polarized wave can rotate in two senses: $\varphi = -\frac{\pi}{2}$ is called the right-hand or clockwise and $\varphi = +\frac{\pi}{2}$ is also called the left-hand or counter clock-wise.

When $E_x \neq E_y$, or $E_x = E_y$ but φ other than 0 or $\pm\frac{\pi}{2}$, equation (5) then becomes [12]

$$\begin{aligned} E(z,t) &= \mathrm{Re}\left[\left(\hat{x}E_x + \hat{y}E_y e^{j\varphi}\right)e^{j\omega t}e^{-jkz}\right] \\ &= \hat{x}E_x \cos(\omega t - kz) + \hat{y}E_y \cos(\omega t - kz + \varphi), \end{aligned} \tag{10}$$

or in a given z plane, say z = 0,

$$\begin{aligned} E_x(z,t) &= E_x \cos\omega t \\ E_y(z,t) &= E_y \cos(\omega t + \varphi)\,. \end{aligned} \tag{11}$$

4. REFLECTION COEFFICIENT AND THE COMPLEX DIELECTRIC CONSTANT

4.1. Reflection coefficient

The Reflection coefficient is a vector quantity that represents the ratio of reflected electric field strength to incident field strength [17].

Mathematically, the reflection coefficient ρ is defined as:

$$\rho = \frac{E_1'}{E_1}, \tag{12}$$

where E_1' is reflection field strength (V/m) in medium 1, E_1 is incident field strength (V/m) in medium 1 [17].

- **S-polarization** [17]
  - The electric field is polarized in perpendicular to the plane of incidence.
  - Parallel to the boundary surface.
- **P-polarization** [17]
  - The electric field is polarized in parallel with the plane of incidence.
  - Perpendicular to the boundary surface.

As shown in Figure 7, the field incident to and reflected from a surface define a plane termed the plane of incidence. If the polarization direction (electric field vector) lies in this plane, the field is termed the p-polarized. If the polarization vector is perpendicular to this plane, the field is the s-polarized. Any intermediate state of polarization is expressed as a vector sum of the s- and p-components. [19]

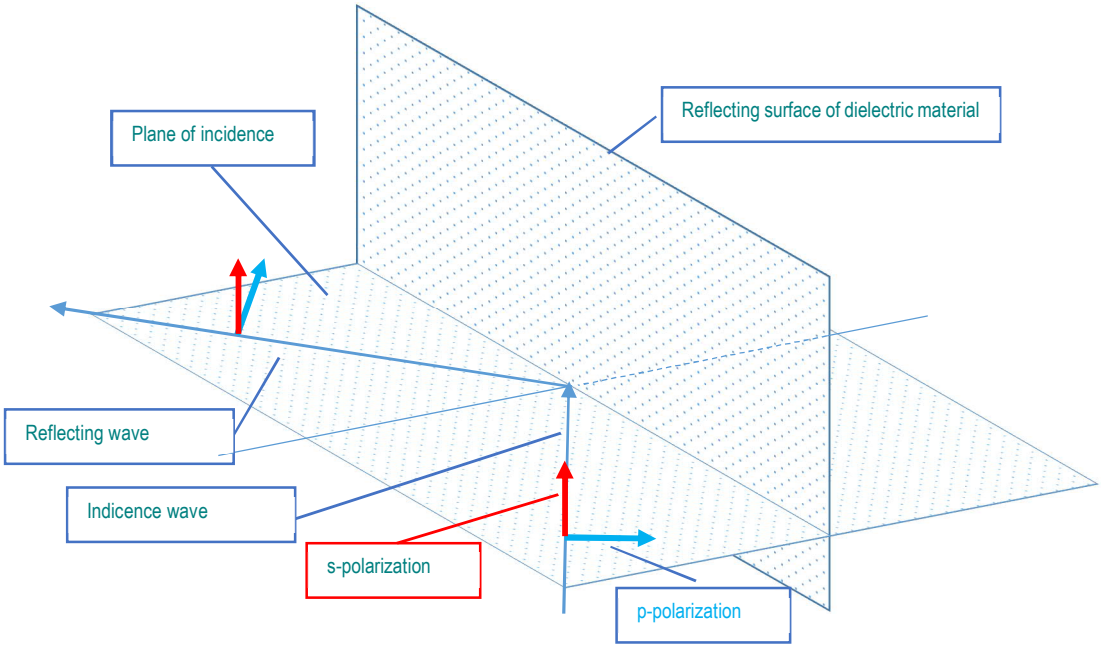

Figure 7. The electric field vector for p-polarized field lies in the plane of incidence, while for s-polarized field, it is perpendicular to the plane of incidence

4.1.1. Reflection coefficient of s-polarization

S-polarization is the perpendicular polarization, where the electric field is perpendicular to the plane of incidence; the magnetic field is in the plane of incidence [22]. The reflection coefficient of s-polarization (⊥ -polarization) can be written as [20]:

$$\rho_{\perp} = \frac{E'_{1,\perp}}{E_{1,\perp}} = \frac{\cos\theta_i - \sqrt{\frac{\varepsilon_2}{\varepsilon_1} - \sin^2\theta_i}}{\cos\theta_i + \sqrt{\frac{\varepsilon_2}{\varepsilon_1} - \sin^2\theta_i}}, \tag{13}$$

where $\rho_{\perp}$ is reflection coefficient of s-polarization (unitless), $E'_{1,\perp}$ is reflection field strength of s-polarization (V/m) in medium 1, $E_{1,\perp}$ is incident field strength of s-polarization(V/m) in medium 1, θ_i is the angle of incidence, ε_1 is permittivity of the medium 1, ε_2 is permittivity of the medium 2.

Figure 8 shows the behaviour of the reflection coefficient as a function of the angle of incidence for both polarizations, when $n_1 < n_2$, that is, $\varepsilon_1 < \varepsilon_2$. In case of the parallel polarization, the reflection coefficient is equal to zero at Brewster's angle as [20]:

$$\theta_B = \arcsin\sqrt{\frac{\varepsilon_2}{\varepsilon_2 + \varepsilon_1}}, \tag{14}$$

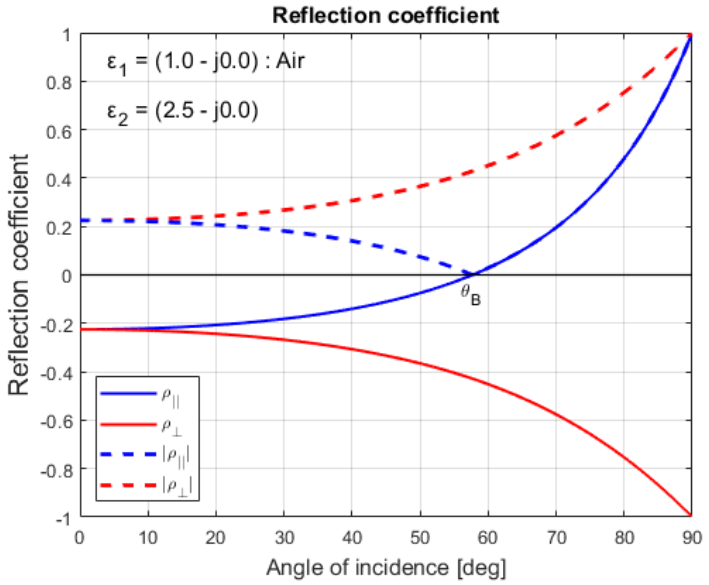

Figure 8. The reflection coefficient for the parallel ($\rho_{\parallel}$) and perpendicular ($\rho_{\perp}$) polarizations as a functions of the angle of incidence θ_1, when $\varepsilon_1 < \varepsilon_2$.

If $\varepsilon_1 > \varepsilon_2$, a total reflection occurs at angles of incidence as:

$$\theta_1 \geq \arcsin\sqrt{\frac{\varepsilon_2}{\varepsilon_1}}\,, \tag{15}$$

Reflection coefficient for a perpendicular polarization (s) using only the incident angle $\varepsilon_1 = 1$ [20].

$$\xrightarrow[\varepsilon_1=1]{} \rho_{\perp} = \frac{\cos\theta_i - \sqrt{\varepsilon_2 - \sin^2\theta_i}}{\cos\theta_i + \sqrt{\varepsilon_2 - \sin^2\theta_i}} \tag{16}$$

$$\begin{aligned}\rho_{\perp} = \frac{E'_{1,\perp}}{E_{1,\perp}} &= \frac{\cos\theta_i - \sqrt{\frac{\varepsilon_2}{\varepsilon_1} - \sin^2\theta_i}}{\cos\theta_i + \sqrt{\frac{\varepsilon_2}{\varepsilon_1} - \sin^2\theta_i}} \\ &= \frac{\cos\theta_i - \sqrt{\frac{\varepsilon_2}{\varepsilon_1}}\cos\theta_t}{\cos\theta_i + \sqrt{\frac{\varepsilon_2}{\varepsilon_1}}\cos\theta_t} \\ &= \frac{\sqrt{\varepsilon_1}\cos\theta_i - \sqrt{\varepsilon_2}\cos\theta_t}{\sqrt{\varepsilon_1}\cos\theta_i + \sqrt{\varepsilon_2}\cos\theta_t}\end{aligned} \tag{17}$$

Reflection coefficient for an s-polarization (perpendicular polarization) using the incident angle and refraction angle [20]

$$\longrightarrow \rho_{\perp} = \frac{n_1 \cos\theta_i - n_2 \cos\theta_t}{n_1 \cos\theta_i + n_2 \cos\theta_t} \ . \tag{18}$$

4.1.2. Reflection coefficient of p-polarization

P-polarization (‖-polarization) is the parallel polarization, where the electric field is parallel to the plane of incidence; then, the magnetic field is normal to the plane of incidence [22].

$$\begin{aligned} \frac{\sin\theta_t}{\sin\theta_i} = \sqrt{\frac{\mu_1\varepsilon_1}{\mu_2\varepsilon_2}} \rightarrow \sin^2\theta_t &= \frac{\varepsilon_1}{\varepsilon_2}\sin^2\theta_i \rightarrow 1 - \sin^2\theta_t \\ &= 1 - \frac{\varepsilon_1}{\varepsilon_2}\sin^2\theta_i \rightarrow \cos^2\theta_t = 1 - \frac{\varepsilon_1}{\varepsilon_2}\sin^2\theta_i \\ &\rightarrow \frac{\varepsilon_2}{\varepsilon_1}\cos^2\theta_t = \frac{\varepsilon_2}{\varepsilon_1} - \sin^2\theta_i \rightarrow \sqrt{\frac{\varepsilon_2}{\varepsilon_1}}\cos\theta_t \\ &= \sqrt{\frac{\varepsilon_2}{\varepsilon_1} - \sin^2\theta_i} \end{aligned} \tag{19}$$

$$\rho_{\parallel} = \frac{E'_{1,\parallel}}{E_{1,\parallel}} = \frac{\sqrt{\frac{\varepsilon_2}{\varepsilon_1} - \sin^2\theta_i} - \frac{\varepsilon_2}{\varepsilon_1}\cos\theta_i}{\sqrt{\frac{\varepsilon_2}{\varepsilon_1} - \sin^2\theta_i} + \frac{\varepsilon_2}{\varepsilon_1}\cos\theta_i} \tag{20}$$

Reflection coefficient for a parallel polarization (p-polarization) is simplified when $\varepsilon_1 = 1$ [20]

$$\xrightarrow[\varepsilon_1=1]{} \rho_{\parallel} = \frac{\sqrt{\varepsilon_2 - \sin^2\theta_i} - \varepsilon_2\cos\theta_i}{\sqrt{\varepsilon_2 - \sin^2\theta_i} + \varepsilon_2\cos\theta_i}. \tag{21}$$

$$\begin{aligned} \rho_{\parallel} &= \frac{E'_{1,\parallel}}{E_{1,\parallel}} \\ &= \frac{\sqrt{\frac{\varepsilon_2}{\varepsilon_1}}\cos\theta_t - \frac{\varepsilon_2}{\varepsilon_1}\cos\theta_i}{\sqrt{\frac{\varepsilon_2}{\varepsilon_1}}\cos\theta_t + \frac{\varepsilon_2}{\varepsilon_1}\cos\theta_i} \quad \overset{\cdot\frac{\varepsilon_1}{\sqrt{\varepsilon_2}}}{=} \quad \frac{\sqrt{\varepsilon_1}\cos\theta_t - \sqrt{\varepsilon_2}\cos\theta_i}{\sqrt{\varepsilon_1}\cos\theta_t + \sqrt{\varepsilon_2}\cos\theta_i} \end{aligned} \tag{22}$$

Reflection coefficient for a p-polarization using incident angle and refraction angle [20].

$$\xrightarrow[\varepsilon_1=1]{} \rho_{\parallel} = \frac{n_1\cos\theta_t - n_2\cos\theta_i}{n_1\cos\theta_t + n_2\cos\theta_i} \tag{23}$$

4.2. Complex dielectric constant

The complex dielectric constant that has a strong dependence from the frequency is a physical quantity that expresses the capability of materials to withstand external fields [21].

During a periodic variation of a sine-shaped electric field, the complex permittivity ε can be expressed as [15]

$$\varepsilon = \varepsilon' - \mathrm{j}\varepsilon'' = \varepsilon_r \varepsilon_0 \,, \tag{24}$$

where ε' is the real part and ε'' is the imaginary part. The ratio of the permittivity of a substance to the permittivity of free space ε_0 is defined by the dielectric constant ε_r.

5. MEASUREMENT TECHNIQUES

The measurements were conducted in a lecture hall on the Linnanmaa campus at the University of Oulu. The measurement targets were two different types of brick walls. Both of the wall were build using perforated bricks. The first wall has the bricks laid on side, producing a fairly smooth surface. The finish has been done with a layer of white paint. The second wall has the bricks laid on edge, so that the perforation is visible, producing a regular grid of open holes leading directly to a fiberglass insulation behind the wall. No finishing has been done on this wall. Both walls are several years old, and the moisture level is the one of the normal indoor air.

5.1. Antennas

An antenna is a basic component that provides the interconnecting links between transmitter and receiver via free space. Here, broadband double-ridged waveguide horn antennas (Rohde & Schwarz HF906) are used. The antenna is made of aluminium and tinned glass-reinforced plastic (GRP) boards to keep its weight low [26]. Figure 9 shows the measurement setup used for recording the reference LOS data that was needed for normalizing the reflection measurement data. Figure 10 shows the orientation of the antennas to produce p-polarized wall reflection. Figure 11 shows the measurement setup used for recording the reflection data of the perforated (red) brick wall.

Figure 9. LOS reference measurement setup.

Figure 10. Orientation of the TX and RX antennas for p-polarization measurement.

Figure 11. Reflection measurement setup, p-polarization.

Table 1. Technical specifications for broadband horn antenna HF906

Property	**Value**
Frequency range	1 to 18 GHz
Typical gain	7 to 14 dBi
Impedance	50 Ω
Maximum continuous power	200 W
Cross polarization	20 dB minimum
Connector	N-type female
Voltage standing wave ratio	Typ. <1.5
Weight	Approx. 1.9 kg
Dimensions (Length×Width×Height)	Approx. 29 cm × 25 cm × 16 cm
Polarization	Linear
Temperature range	0 °C to +50 °C

5.2. Scattering parameters

As described in the Keysight manual [28], the calibration data are calculated by connecting an OPEN standard, a LOAD standard. The scattering parameter (s-parameter) matrix contains the reflection and transmission coefficients between the input and output ports of a system. A two-port device has four s-parameters. The first sub-index is the port where the signal is measured, and the second sub-index is the port where the signal is generated. As explained in Figure 12, S_{21} is a part of the signal measured in port 2 relative to the radio frequency (RF) stimulus coming out from port 1 at the defined point frequencies. When the sub-indices are the same (e.g., S_{11}), the measured quantity is a reflection coefficient, when the input and output ports are the same.

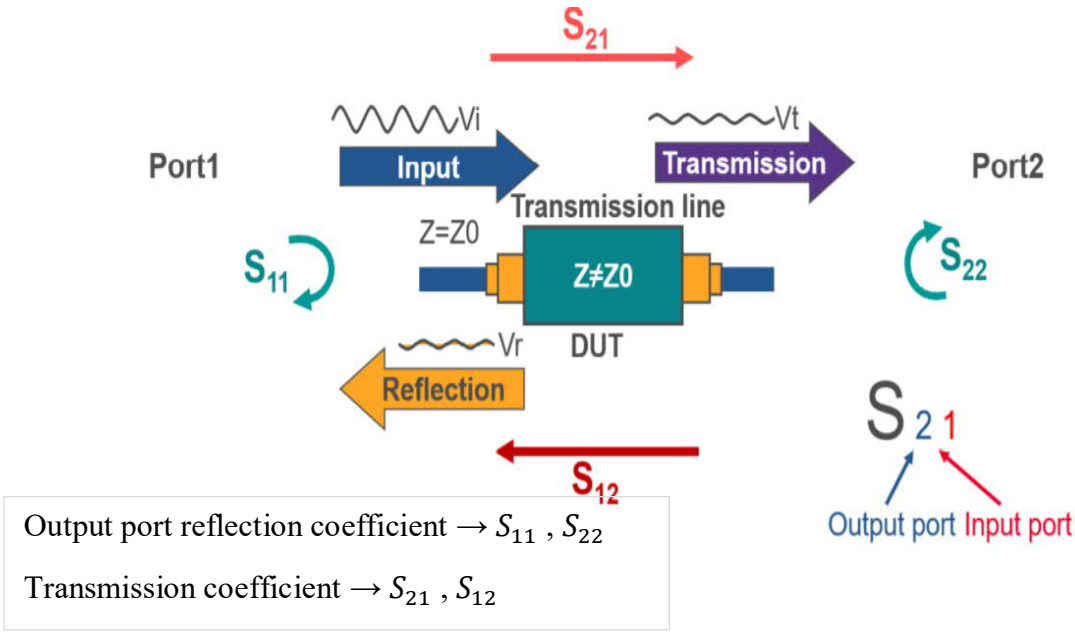

Figure 12. S-parameters form a complex matrix that show reflection/transmission characteristics (amplitude/phase) in frequency domain.

5.3. Network analyzer

A network analyzer is an equipment that measures the network parameters of electrical networks. Network analyzers are often used to represent two-port systems such as amplifiers and filters, although network analyzer can be used on systems with an arbitrary number of ports. Network analyzers are mostly used at high frequency ranges up to 1.05 THz. Particular types of network analyzers can also cover lower frequency ranges down to 1 Hz [23].

The two types of network analyzers are:

- **Scalar network analyzer** (SNA)—measures amplitude properties only. An SNA is functionally identic to a spectrum analyzer in combination with a tracking generator.
- **Vector network analyzer** (VNA)—measures of both amplitude and phase properties.

VNA-based measurement system

Vector network analyzer (VNA) is one of the best instruments in radio engineering and applications. A VNA may also be called an automatic network analyzer or a gain-phase meter. The VNA is popular for its accuracy and high dynamic range [23]. The VNA is a test system that enables the microwave devices to be characterized in terms of network scattering parameters, or s-parameters, and the RF performance of radio frequency band. The VNA characterizes high-frequency passive and active devices in their linear mode of operation by measuring their s-parameters as functions of frequency. In this study, the HP 8720ES s-parameter network analyzer shown in Figure 13 was used.

Figure 13. 8720ES network analyzer [27].

Table 2. Properties of 8720ES network analyzer.

Property	**Value**
Frequency range	50 MHz to 20 GHz
Number of frequency points	up to 1601
Output power level	+5 to -70 dBm
Dynamic range	93 dB
Resolution	1 Hz
Colour screen	TFT
Integrated connectors	3.5mm

5.4. Calibration

A vector network analyzer reaches accurate measurements by correcting for the characteristics of cables and systematic errors in the instrument. The process of error correction is commonly called calibration, sometimes user-calibration to indicate the difference from periodic calibration executed by the manufacturer. Calibration commonly involves measuring known standards and using those measurements to pay for systematic errors [23].

Full 2-Port Calibration

In full 2-port calibration, as described in Figure 14, and as explained in the calibration manual [25], the calibration data are calculated by connecting an OPEN standard, a LOAD standard or a SHORT standard to two desired test ports. This calibration effectively eliminates the directivity error, source match error, frequency response reflection tracking error, frequency response transmission tracking error, and crosstalk. This calibration enables performing measurements with the highest possible accuracy.

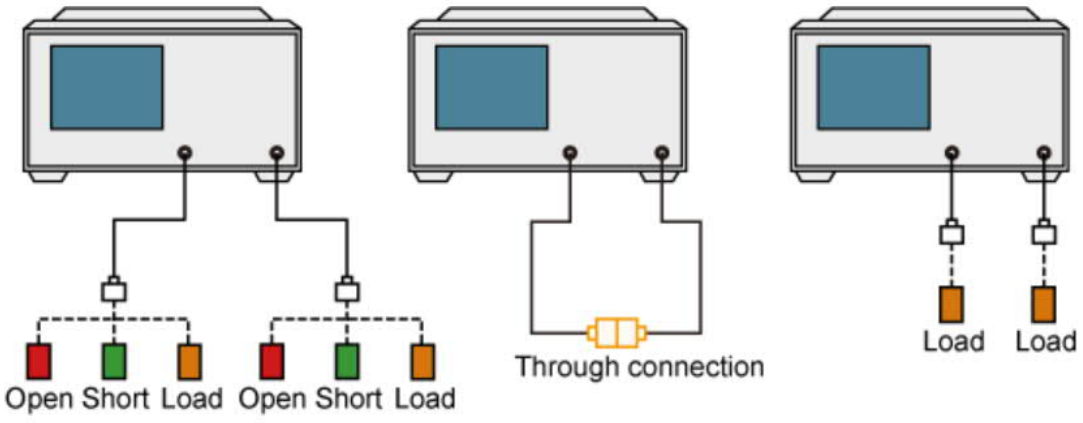

Figure 14. Connecting standards in full 2-port calibration [25].

5.4.1 Calibration kits

The Agilent 85032B (Figure 15) and 85032E N-type calibration kits are used to calibrate Agilent network analyzers up to 6 GHz for measurements of components with 50Ω N-type connectors.

The calibration kit 85032F contains precision 50 Ω type-N standards used to calibrate network analyzers. The kit includes fixed terminations, open circuits, short circuits, broadband loads, and adapters. This calibration kit is specified from DC to 9 GHz [24].

The 85032B calibration kit contains the following [18]:
• one male and one female open termination
• one male and one female short termination
• one male and one female 50Ω load
• two type-N-male to 7-mm adapters (included with Option 100)
• two type-N-fe7*male to 7-mm adapters (included with Option 100).

Keysight / Agilent 85032B Type-N calibration kit includes [24]:

- Open, Type-N Female (85032-60012)
- Open, Type-N Male (85032-60007)
- Short, Type-N Female (85032-60009)
- Short, Type-N Male (85032-60008)
- Termination, Type-N Male 50 Ω (00909-60009)
- Termination, Type-N Female 50 Ω (00909-600010)
- Adapters and Spare parts.

Figure 15. Keysight / Agilent 85032B Type-N calibration kit.

5.4.2. 3.5 mm calibration kit

The 3.5 mm calibration kit 85052B contains precision standards to characterize the systematic errors at frequency range from DC to 26.5 GHz. This kit also contains torque wrenches for properly connecting standards, adapters to change the sex of the test port, and connector gauges for verifying and maintaining the connector interface [10]. The 3.5 mm connector is mechanically compatible with the SMA connector.

5.5. Measurement setup

The key concept is to utilizing vector network analyzer (VNA) for measuring different material properties. The measurement system consisted of a VNA (8720ES), two Rohde & Schwarz HF906 horn antennas as TX and RX, and RF cables are used for this setup.

Table 3. Measurement parameters for the lower frequency band measurements.

Property	**Value**
Frequency range	1 – 9.5 GHz
Number of points	1601
Power level	+5 dBm

Table 4. Measurement parameters for the higher frequency band measurements.

Property	**Value**
Frequency range	9.5 – 18 GHz
Number of points	1601
Power level	+5 dBm

GPIB interface is used to connect the VNA with a laptop and to collect and store the data for later analysis with Matlab™.

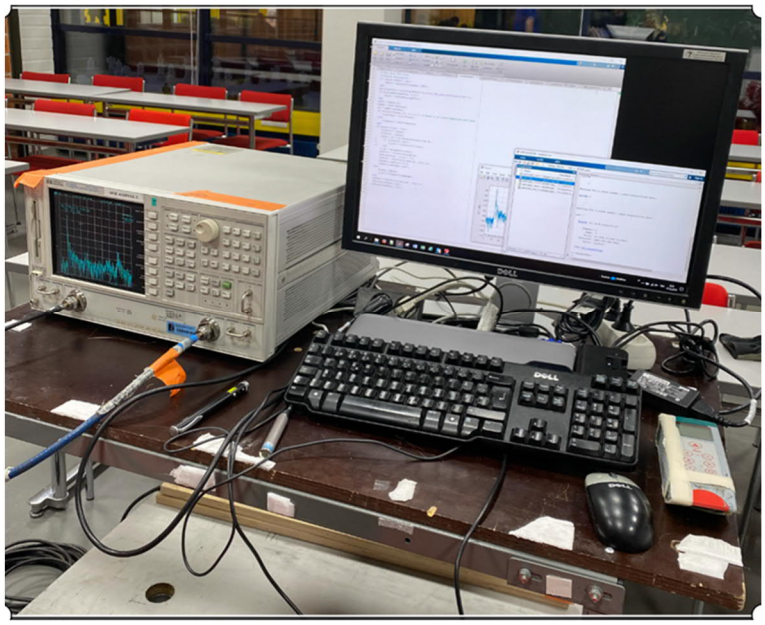

Figure 16. The measurement setup in the operation.

6. MEASUREMENT SCENARIOS AND ANALYSIS METHOD

Reflection measurements were performed in the lecture room PR102 at the University of Oulu. These measurements were necessary to calculate the complex dielectric constant of several surfaces. The measurement setup is described in Chapter 5. The LOS reference measurement was done with an antenna separation of 3.2 m. The height of the antenna from the ground was 1.30 m. It was enough to measure a single linear polarization in the experiment because the concept of (pseudo) Brester's angle exists only for the p-polarized interaction. The absolute value of reflection coefficient is calculated by normalizing the received reflected electric field strength with the received field strength of reference LOS measurement. The propagation path difference is compensated by dividing the reflected path length $d_1 + d_2$ by the reference path length d_{LOS}. The reflection coefficient is thus calculated by [16]:

$$| \rho | = \frac{d_1 + d_2}{d_{LOS}} \sqrt{\frac{P_{refl}}{P_{LOS}}} \quad . \tag{25}$$

Before applying (25), the measured power levels are converted into the linear scale by transform $P = 10^{P_{dB}/10}$.

Figure 17 shows the surface reflection in a general case and the practical view of the measurement system in different scenarios. Distance d_{LOS} is the length of the reference line-of-sight (LOS) path between TX_{LOS} and RX_{LOS}. Distance d_0 is the 3D distance between the transmitter and the receiver. Distance d_{01} is the separation of TX_x and RX_x in direction x. Distance d_1 is the distance from the transmitter to the reflection point and d_2 is the distance from the reflection point to the receiver. Angle θ_i is the angle of incidence. Distances d_A and d_B are the distances between the transmitter and the reflection wall, and between the receiver and the reflection wall, respectively. RX' is the mirror image of the receiver.

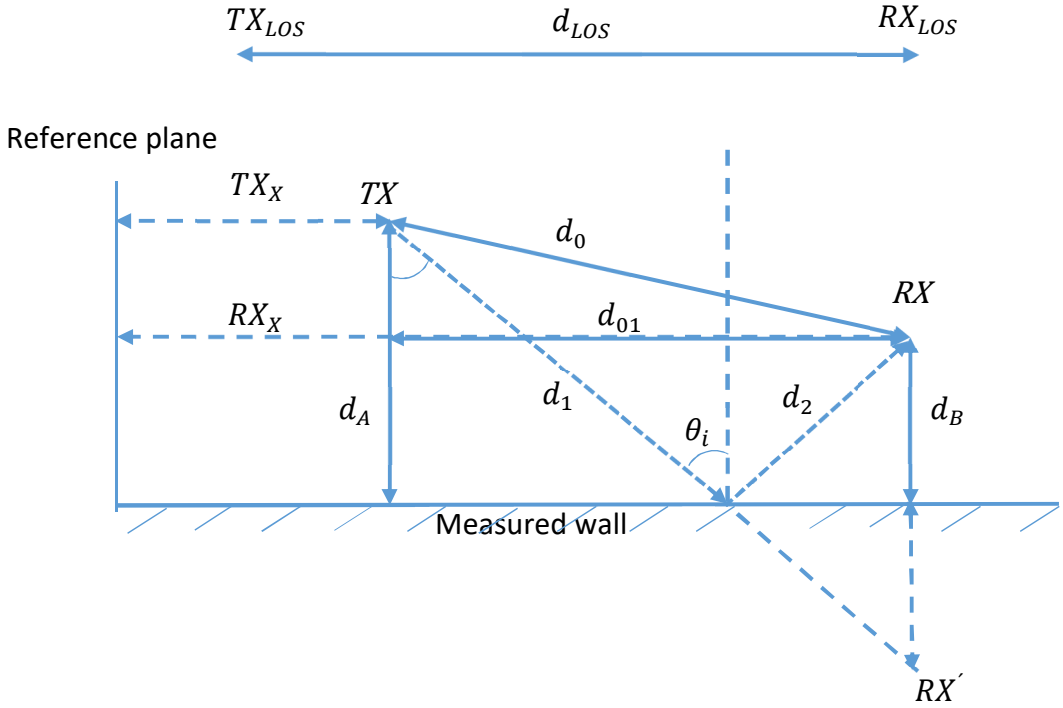

Figure 17. Surface reflection in a general case.

From Figure 17, the total length of the reflected path can be defined as:

$$d_1 + d_2 = \sqrt{(d_A + d_B)^2 + d_{01}^2}\,, \tag{26}$$

where d_{01} is calculated by the X-distance difference of TX and RX as

$$d_{01} = RX_X - TX_X\,. \tag{27}$$

The angle of incidence is given by

$$\theta_i = \arcsin\left(\frac{d_{01}}{d_1 + d_2}\right). \tag{28}$$

The complex dielectric constant ε_r is found by fitting the absolute value of the theoretical reflection coefficient curve (20) in the p-polarization data and using minimum root mean square error (RMSE) as the fitting criterion. RMSE is calculated as [14]

$$\text{RMSE} = \sqrt{\frac{1}{n}\sum_{i=1}^{n}\left(Y_i - \hat{Y}_i\right)^2}\,, \tag{29}$$

where Y_i is the sample value, $\hat{Y}_i$ is the estimation value and n is the number of sample values.

A Matlab™ routine developed within the Centre for Wireless Communication is utilized in analysing the measurement results. Figures from Figure 18 through Figure 20 show an example of the curve fitting and RMSE estimation processes. Range of variation $\Delta\varepsilon_r$ is drawn from lower and upper bounds of $\Delta\varepsilon_r$ when the RMSE deviation is less than 0.02.

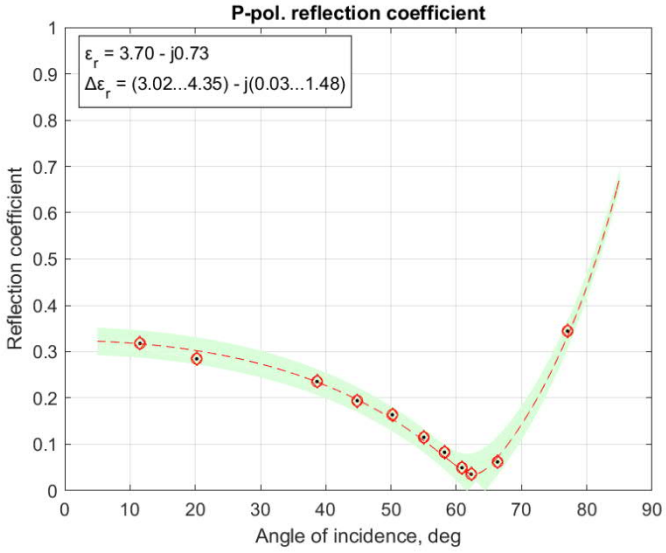

Figure 18. The absolute value of the reflection coefficient graph for p-polarization at 1-9.5 GHz frequency range.

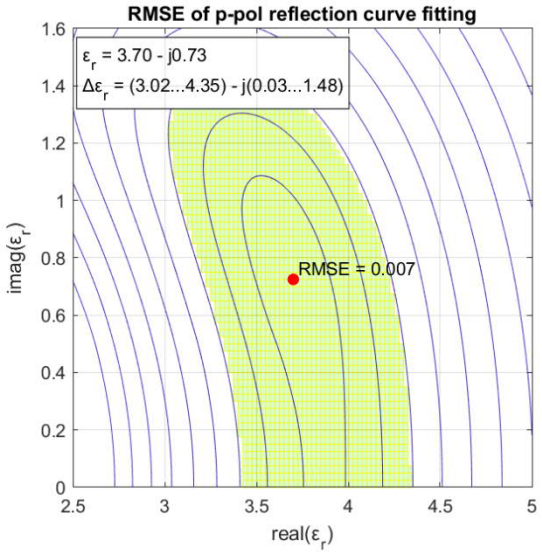

Figure 19. RMSE of p-polarization reflection curve fitting at 1-9.5 GHz frequency range.

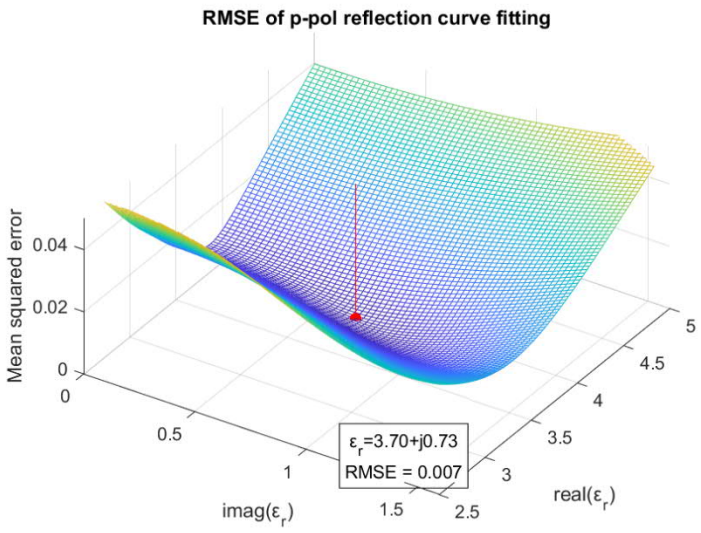

Figure 20. RMSE of p-polarization reflection curve fitting at 1-9.5 GHz frequency range.

7. MEASUREMENT RESULTS

The measurement is done in the upper and lower frequency bands. The upper band is from 9.5 – 18 GHz and the lower band is from 1.0 – 9.5 GHz. The lower frequency band measurement is done in 1601 the number of points and centre of frequency is 5.25 GHz. The lower frequency band measurement was performed in the PR 102 white and a red brick wall at the University of Oulu. Lower frequency band measurements carried out on December 17. The upper-frequency band measurement was performed in the PR 102 white and a red brick wall at the University of Oulu. The upper-frequency band measurements carried out on March 4 and March 5, 2020.

Figure 21 shows the LOS reference signal at 1.0 – 9.5 GHz frequency range. The LOS path length is 3.20 m. The LOS reference path delay is 10.7 ns, and the respective power is -34.2 dB.

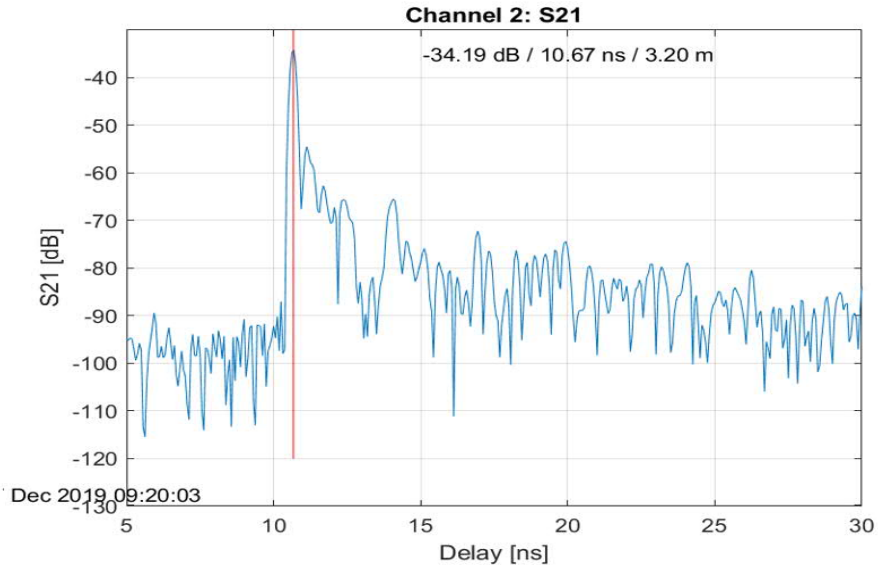

Figure 21. The LOS reference to the white brick wall at 1.0 – 9.5 GHz frequency range.

Figure 22 shows a sample reflection data for p-polarization from the white brick wall at 1.0-9.5 GHz frequency range. The LOS path generated by the side lobes of the antennas during the reflection measurements is ignored in the analysis phase. The wall reflection path length is 5.10 m, the path delay is 17.0 ns, and the respective power is -50.6 dB. The second significant reflection at 20.0 ns is related to a floor-wall corner reflection, which is not within the scope of this work. Similar impulse responses are available for each of the 43 measurement points, and the results are collected in tables from Table 5 through Table 8.

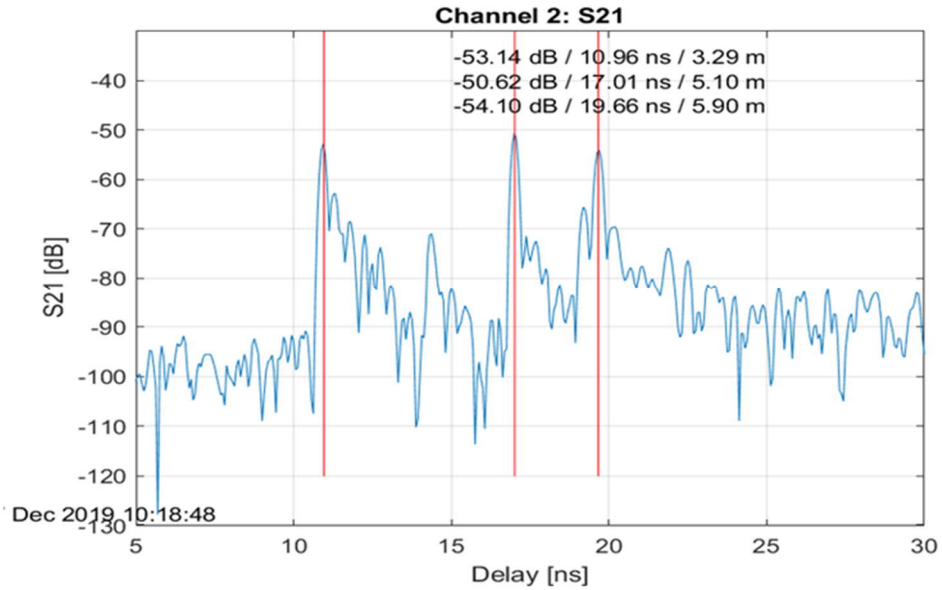

Figure 22. The p-polarization of white brick wall reflection at 1.0 – 9.5 GHz frequency range.

Table 5 shows the immediate lower frequency band measurement results for the white brick wall in PR102 (cf. Figure 11). Notice that the first row contains the values for the reference LOS measurement.

Table 5. The lower frequency band measurement results of the white brick wall in PR102.

File ID	TX_X	TX_Y	RX_X	RX_Y	d_{01}	θ_i	d_1+d_2	P_{db}	$\lvert\rho\rvert$
0920	*3.90*	*1.91*	*7.18*	*1.90*	*3.28*	--	--	*-34.19*	--
1018	3.96	2.00	7.16	2.00	3.20	38.7	5.12	-50.62	0.24
1036	4.67	2.39	6.43	2.39	1.76	20.2	5.09	-48.93	0.28
1044	5.05	2.45	6.05	2.45	1.00	11.5	5.00	-47.81	0.32
1052	4.05	1.50	7.03	1.50	2.98	44.8	4.23	-50.63	0.19
1057	3.83	1.20	7.26	1.20	3.43	55.0	4.19	-55.09	0.12
1102	3.92	1.35	7.16	1.35	3.24	50.2	4.22	-52.09	0.16
1113	3.77	0.91	7.31	0.95	3.54	62.3	4.00	-64.89	0.04
1121	3.60	0.45	7.51	0.45	3.91	77.0	4.01	-45.20	0.34
1127	3.68	0.82	7.42	0.82	3.74	66.3	4.08	-60.25	0.06
1132	3.81	1.07	7.26	1.07	3.45	58.2	4.06	-57.69	0.08
1137	3.76	1.01	7.33	0.98	3.57	60.9	4.09	-62.19	0.05

Table 6 shows the immediate higher frequency band measurement results for the white brick wall in PR102 (cf. Figure 11). Notice that the first row contains the values for the reference LOS measurement.

Table 6. The higher frequency band Measurement results of the white brick wall in PR102.

File ID	TX_X	TX_Y	RX_X	RX_Y	d_{01}	θ_i	d_1+d_2	P_{db}	$\|\rho\|$
1033	*4.75*	*2.28*	*8.92*	*2.30*	*4.17*	--	--	*-40.31*	--
1047	6.41	2.39	7.57	2.37	1.16	13.70	4.90	-51.41	0.3273
1106	5.42	1.24	8.59	1.24	3.17	51.96	4.02	-55.90	0.1604
1113	5.22	0.94	8.77	0.94	3.55	62.10	4.02	-72.46	0.0238
1120	5.24	0.53	8.80	0.52	3.56	73.57	3.71	-53.84	0.1875
1129	5.27	0.66	8.72	0.65	3.45	69.21	3.69	-58.07	0.1145
1135	5.29	0.75	8.74	0.75	3.45	66.50	3.76	-69.68	0.0307
1140	5.29	0.85	8.73	0.84	3.44	63.84	3.83	-93.56	0.0020
1150	5.93	2.10	8.05	2.10	2.12	26.78	4.70	-51.57	0.3086

Table 7 shows the immediate lower frequency band measurement results for the red brick wall in PR102 (cf. Figure 11). Notice that the first row contains the values for the reference LOS measurement.

Table 7. The lower frequency band measurement results of the red brick wall in PR102.

File ID	TX_X	TX_Y	RX_X	RX_Y	d_{01}	θ_i	d_1+d_2	P_{db}	$\|\rho\|$
1045	*4.88*	*2.12*	*8.95*	*2.14*	*4.07*	--	--	*-36.57*	--
1116	4.92	2.14	7.76	2.13	2.84	33.63	5.13	-54.38	0.1621
1133	4.53	1.21	8.16	1.22	3.63	56.20	4.37	-57.95	0.0916
1147	4.63	1.28	8.10	1.29	3.47	53.48	4.32	-65.47	0.0381
1159	4.57	1.14	8.11	1.14	3.54	57.22	4.21	-56.96	0.0989
1210	4.50	0.41	8.17	0.41	3.67	77.41	3.76	-43.65	0.4089
1220	4.53	0.54	8.15	0.54	3.62	73.39	3.78	-46.13	0.3088
1230	4.95	0.63	7.74	0.64	2.79	65.53	3.07	-52.86	0.1155
1243	5.13	0.75	7.54	0.75	2.41	58.10	2.84	-57.35	0.0638
1256	5.19	1.16	7.49	1.15	2.30	44.88	3.26	-53.18	0.1183
1304	6.06	1.85	6.62	1.84	0.56	8.63	3.73	-48.47	0.2330
1315	4.87	0.64	7.81	0.63	2.94	66.64	3.20	-52.07	0.1321
1323	4.95	0.48	7.73	0.48	2.78	70.95	2.94	-45.39	0.2618

Table 8 shows the immediate upper-frequency band measurement results for the red brick wall in PR102 (cf. Figure 11). Notice that the first row contains the values for the reference LOS measurement.

Table 8. The upper-frequency band measurement results of the red brick wall in PR102.

File ID	TX_X	TX_Y	RX_X	RX_Y	d_{01}	θ_i	d_1+d_2	P_{db}	$\|\rho\|$
1057	*4.88*	*2.12*	*8.95*	*2.14*	*4.07*	--	--	*-40.58*	--
1117	4.92	2.14	7.76	2.13	2.84	33.63	5.13	-58.32	0.1633
1136	4.53	1.21	8.16	1.22	3.63	56.20	4.37	-67.99	0.0457
1150	4.63	1.28	8.10	1.29	3.47	53.48	4.32	-69.09	0.0398
1201	4.57	1.14	8.11	1.14	3.54	57.22	4.21	-69.78	0.0358
1212	4.50	0.41	8.17	0.41	3.67	77.41	3.76	-43.74	0.6414
1225	4.53	0.54	8.15	0.54	3.62	73.39	3.78	-51.34	0.2686
1233	4.95	0.63	7.74	0.64	2.79	65.53	3.07	-58.69	0.0935
1248	5.13	0.75	7.54	0.75	2.41	58.10	2.84	-65.69	0.0387
1259	5.19	1.16	7.49	1.15	2.30	44.88	3.26	-56.78	0.1239
1307	6.06	1.85	6.62	1.84	0.56	8.63	3.73	-53.72	0.2018
1318	4.87	0.64	7.81	0.63	2.94	66.64	3.20	-57.11	0.1172
1328	4.95	0.48	7.73	0.48	2.78	70.95	2.94	-51.29	0.2103

The final results for the complex dielectric constant with a variability values are shown in Table 9. The data for frequency range 1-18 GHz is obtained by combining the results of the two sub-bands. The variability $\Delta\varepsilon_r$ is based on fitting curves with the mean square-root error less than 0.02. The curve fitting results are collected in Appendix 1.

The estimated values of dielectric properties of investigated materials are compared with the values found in various scientific publications. The value of complex dielectric constant in range of (3.7-4.22)-j (0.73-0.03) was found to be in accordance with results published by the International Telecommunications Union [2]. However, compared to the result 3.75-j0.0 published in [2], there is some uncertainty in assessing the imaginary part of the dielectric constant.

Table 9: Complex dielectric constants

Material	**1-9.5 GHz**	**9.5-18 GHz**	**1-18 GHz**
Perforated brick - walled up flat - painted white	$\varepsilon_r = 3.70 - j0.73$ $\Delta\varepsilon_{r,real} = (3.02\ldots4.35)$ $\Delta\varepsilon_{r,imag} = j(0.03\ldots1.48)$	$\varepsilon_r = 4.22 - j0.03$ $\Delta\varepsilon_{r,real} = (3.67 \ldots 4.85)$ $\Delta\varepsilon_{r,imag} = j(0.03 \ldots 0.93)$	$\varepsilon_r = 4.00 - j0.03$ $\Delta\varepsilon_{r,real} = (3.50\ldots4.47)$ $\Delta\varepsilon_{r,imag} = j(0.03\ldots1.10)$
Perforated brick - perforation visible - untreated surface	$\varepsilon_r = 2.05 - j0.95$ $\Delta\varepsilon_{r,real} = (1.80\ldots2.40)$ $\Delta\varepsilon_{r,imag} = j(0.78\ldots1.13)$	$\varepsilon_r = 2.35 - j0.50$ $\Delta\varepsilon_{r,real} = (1.95\ldots2.85)$ $\Delta\varepsilon_{r,imag} = j(0.03\ldots0.88)$	$\varepsilon_r = 2.23 - j0.78$ $\Delta\varepsilon_{r,real} = (1.82\ldots2.80)$ $\Delta\varepsilon_{r,imag} = j(0.03\ldots1.07)$
Variation $\Delta\varepsilon_r$ is based on RMSE ≤ 0.02			

8. DISCUSSION

Vector network analyzer (VNA) is a measuring device that is used to measure complex dielectric constant of indoor walls. In this thesis reflection coefficient was measured by using both higher and lower frequency bands with the help of vector network analyzer. VNAs are normally used in field operations to verify and troubleshoot deployed RF and microwave systems. In this experiment, the VNA was used to measure the reflected signal strength over a radio propagation path. The antenna positions were recorded with respect to the wall surface to find out the angle of incidence, and thereafter measured the transmission s-parameter (S_{12}) by using VNA and two horn antennas in a p-polarization orientation. Several angles of incidence over the frequency range of 1-18 GHz were covered in the measurement experiment. The p-polarization reflection coefficient graphs were obtained as functions of the angle of incidence by taking the squared ratio of the reflected path over the reference line-of-sight path power. The LOS path power was previously recorded immediately the calibration procedures were completed. The travel path difference was compensated by taking into account the ratio of the paths.

The reflection measurements were performed of two different walls that were built using perforated bricks in lecture room PR102 at the University of Oulu. The first wall was walled up on flat side of the bricks, and the finish was white paint. The second wall was walled up on the short side of the bricks, and there was no finish on the surface revealing the perforation of the bricks.

Only the p-polarization data were collected in the measurements. Adding measurement results of perpendicular polarization (s-polarization) would have doubled the amount of work, but not significantly adding confidence in the fitting process. Thanks to the characteristic Brewster's angle appearing at p-polarization, the fitting results are accurate enough without having the s-polarization data. If there were a 4-port VNA and dual-polarized antennas at hand, measurements at s-polarization would have been justified.

Efficient planning before the measurement is very crucial for the accuracy of the analysis. The planning includes selection of antennas having a distinct main beam pattern. Also, selection of the reference coordinate system for recording the exact antenna positions is important, so that the angle of incidence can be reliably calculated. The antenna positions can be selected more or less freely, but having the antennas directed symmetrically at equal distances towards a selected target spot on the wall ensures that all measurements are taken from the same reflection point. The full 2-port calibration selected as the user calibration method ensured successful measurements. The measurement parameters were chosen carefully to enable unaliased impulse responses and a good delay resolution for extraction of the reflected path power.

The estimated values of dielectric properties of investigated materials are compared with the values found in various scientific publications. There is some uncertainty in assessing the imaginary part of the dielectric constant.

A theoretical model is implemented, so that the minimum difference between the theoretical and measured absolute value of reflection coefficient gives an estimated value of complex relative permittivity. The real and imaginary part of complex relative permittivity is investigated in this thesis. The real part signifies the amount of electric energy stored in a material and is called dielectric constant whereas the imaginary part

is called the loss factor, which signifies the dissipation of the radiated energy. The dielectric constants of insulating solids can be noticeably changed by absorbed moisture.

The results show a mild frequency dependency of the complex dielectric constant, so that the imaginary part is smaller at the higher frequency band in both of the wall types. At the same time the real part gets larger at the higher frequency. There is a clear difference in the real part of the dielectric constant between the walls, but since the uncertainty of the imaginary part is significant, no judgement of the absorption properties of the walls can the stated. On the other hand, the variability range of the lowest and highest frequencies in this measurement was too low to judge any estimation of the complex dielectric constant at mm-wave frequencies.

The measurement system was able to perform efficiently for the proposed objective of the study. However, several improvements can be made in future to adopt more accurate measurement system to study the reflection characteristics of building materials. Analysis software integrated with the reflection data collection would make the assessment of dielectric constants faster in the future. For the user, this would allow changing parameters while measuring and thus be able to improve the results. Using an accurate robotic positioner to move the antenna would speed up the measurement. Automated reading of antenna position would make the calculation of angle of incidence more accurate.

Observing the above scenarios, one can decide that the assessment process is able provide the desired results. Finally, it can be said that the experiment is successfully done.

9. SUMMARY

The goal of this thesis is to utilize vector network analyzer for measuring material properties by inspecting the reflection of an electromagnetic wave from a flat surface of a material sample. The measurement setup utilized a two-port VNA, and two linear polarized horn antennas. The setup is controlled by a laptop, and the data is collected by a control software. The experiments were done in the lecture room PR102 at the University of Oulu. The antennas were directed to a common spot on the target wall to measure the reflection coefficient. Various scenarios were created during the experiments, and their results are evaluated. Finally, the assessment of complex dielectric constant is done with the help of the Brester's angle and reflection coefficient.

A Matlab™ routine developed within the Centre for Wireless Communication is utilized in analysing the measurement results. The reflection coefficients were estimated from the measured data taking into account the increased attenuation due a longer path length. After applying the path length compensation, coefficients falling within one degree from each other are averaged to give the data equal weighing over the abscissa. Finally, the theoretical curve of the reflection coefficient is fitted on the data.

REFERENCES

[1] Ivan Vilovic, Niksa Burum and Robert Nadj, "Estimation of dielectric constant of composite materials in buildings using reflected fields and PSO algorithm," *Fourth European Conference on Antennas and Propagation,* Barcelona, Spain, May, 2010, pp. 1-5.

[2] ITU-R, "*Recommendation P.2040-1: Effects of building materials and structures on radiowave propagation above about 100 MHz*", International Telecommunication Union, July 2015

[3] Murat Torlak, "Telecommunication Switching & Transmission (EE4367)", University of Texas at Dallas (UTD), March 18, 2008.

[4] Propagation Overview, (accessed 25 November 2019), [Online]. URL: https://www.electronics-notes.com/articles/antennas-propagation/propagation-overview/basics.php.

[5] Path loss, (accessed 25 November 2019), [Online]. URL: https://en.wikipedia.org/wiki/Path_loss.

[6] RFID Link Budget Formula, (accessed 25 December 2019), [Online]. URL: https://electronics.stackexchange.com/questions/437528/rfid-link-budget-formula.

[7] Reflection and Refraction ,2006 Encyclopaedia Britannica, Inc, (accessed 25 October 2019), [Online]. URL: https://www.britannica.com/science/light/Reflection-and-refraction.

[8] Pankaj Chakrabarty, *"Validation of measurement setup for assessing complex dielectric constant",* Master's thesis, University of Oulu, 2019.

[9] Ankit Regmi, *"Reflection measurement of building materials at microwaves",* Master's thesis, University of Oulu, 2016.

[10] Keysight Technologies, "85052B 3.5 mm Calibration Kit", (accessed 16 March 2020), [Online]. URL: https://www.libertytest.com/store/viewPrd.asp?idCategory=24&opt=2&idProduct=1218.

[11] Ming Lu, T. Lo, J. Litva, "A Physical Spatio-Temporal Model of Multipath Propagation Channels", *IEEE 47th Vehicular Technology Conference, Technology in Motion*, May 4-7, 1997.

[12] Simon Ramo, John R. Whinnery, Theodore Van Duzer, *"Fields and Waves In Communication Electronics",* John Wiley & Sons, Inc., 3rd Edition, August 1993, pp. 280-282.

[13] Polarization (Waves), (accessed 25 December 2019), [Online]. URL: https://en.wikipedia.org/wiki/Polarization_(waves).

[14] B. Sridhar and M. Z. A. Khan, "RMSE comparison of path loss models for UHF/VHF bands in India," 2014 IEEE region 10 symposium, pp. 330-335, 15 01 2014.

[15] Jonas Alin, PhD Polymer Science & Materials Chemistry, Royal Institute of Technology (2012), updated Oct 4,2019. (accessed 25 October 2019), [Online]. URL: https://www.quora.com/what -is-the-complex-dielectric-constant.

[16] O. Landron, M. J. Feuerstein and T. S. Rappaport, "A comparison of theoretical and empirical reflection coefficients for typical exterior wall surfaces in a mobile radio environment," in *IEEE Transactions on Antennas and Propagation,* vol. 44, no. 3, pp. 341-351, Mar 1996.

[17] Eugene Hecht, Adelphi University, "Optics", Addison- Wesley, 4th edition, August 2001.

[18] Calibration Kit Overview, "Agilent 85032B Calibration Kits", (accessed 8 February 2020), [Online].
URL: https://www.instrumex.de/datasheet/85032B_E.pdf.

[19] S-polarization and P-polarization, (accessed 20 January 2020), [Online]. URL: https://www.photonics.com/Articles/ThinFilm_Coatings_A_Buyers_Guide/a42399.

[20] Antti V. Räisänen, Arto Lehto, *"Radio Engineering For Wireless Communication And Sensor Applications",* Artech House, Inc. Boston. London, 2003, pp.31.

[21] Complex dielectric constant, (accessed 20 November 2019), [Online]. URL: https://study.com/academy/answer/what-is-the-complex-dielectric-constant.html.

[22] Fresnel equations, (accessed 29 October 2019), [Online]. URL: https://en.wikipedia.org/wiki/Fresnel_equations.

[23] Network Analyzer, (accessed 6 February 2020), [Online]. URL: https://en.wikipedia.org/wiki/Network_analyzer_(electrical).

[24] 85032F Standard Mechanical Calibration Kit, DC to 9 GHz, Type-N, 50 ohms, (accessed 15 January 2020), [Online]. URL:https://www.keysight.com/en/pd-1000003537%3Aepsg%3Apro-pn-85032F/standard-mechanical-calibration-kit-dc-to-9-ghz-type-n-50-ohm?nid=-32574.536880667&cc=F.

[25] Full 2-port calibration, (accessed 10 March 2020), [Online]. URL: http://ena.support.keysight.com/e5071c/manuals/webhelp/eng/measurement/calibration/basic_calibrations/full_2_port_calibration.htm.

[26] SHF Antennas, "Double-Ridged Waveguide Horn Antenna, HF 906 pdf ", (accessed 20 January 2020), [Online]. URL: https://cdn.rohde-schwarz.com/pws/dl_downloads/dl_common_library/dl_brochures_and_datasheets/pdf_1/HF906_brief_e.pdf.

[27] Keysight or Agilent, "8720ES S- parameter network analyzer", (accessed 10 January 2020), [Online]. URL: http://en.leasametric.com/search/8720/726/keysight-agilent-8720es.

[28] S-parameter, (accessed 26 January 2020), [Online]. URL: http://literature.cdn.keysight.com/litweb/pdf/5991-3736EN.pdf.

APPENDIX

Appendix 1. The curve fitting results

Figures from Figure 23 through Figure 25 show the complex dielectric constant of the brick wall (painted perforated bricks, walled up flat) in PR102. Figures show the curve fitting and RMSE estimation results. Variation of the reflection coefficient is drawn using $\Delta\varepsilon_r$ from the range where RMSE<0.02.

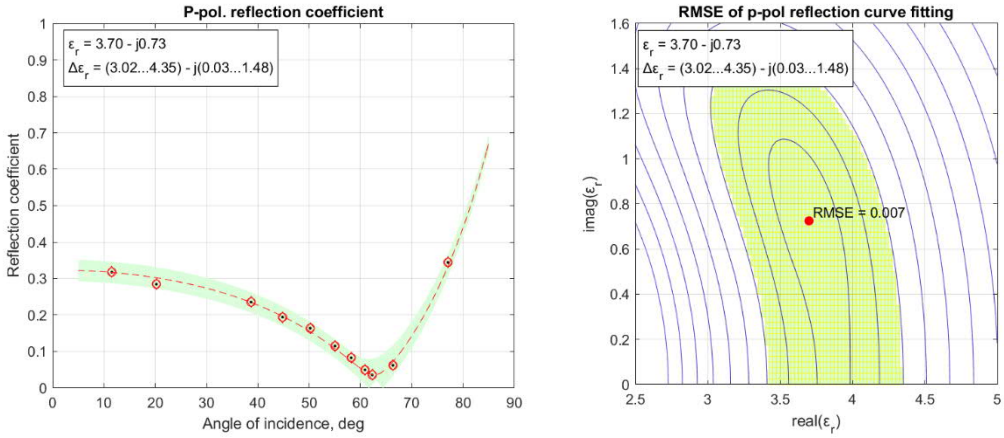

\

Figure 23: PR102 (white brick wall) at 1-9.5 GHz frequency range, RMSE<0.02.

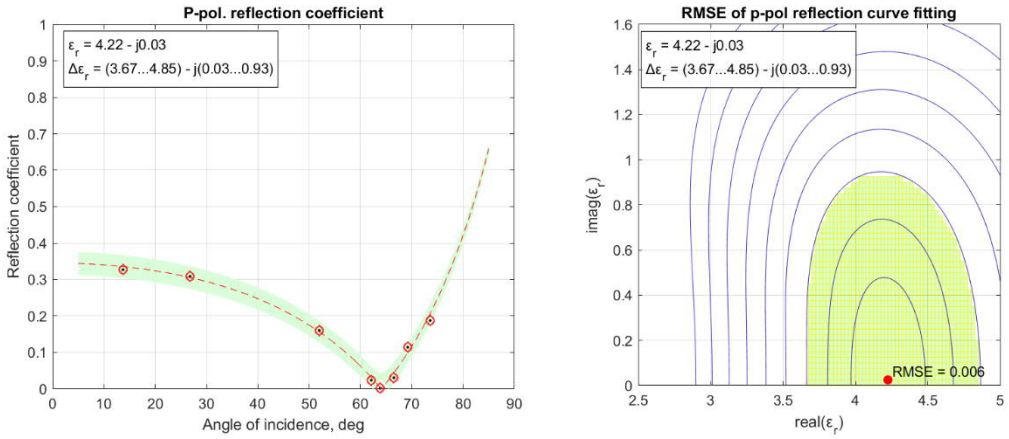

Figure 24: PR102 (white brick wall) at 9.5-18 GHz frequency range, RMSE<0.02.

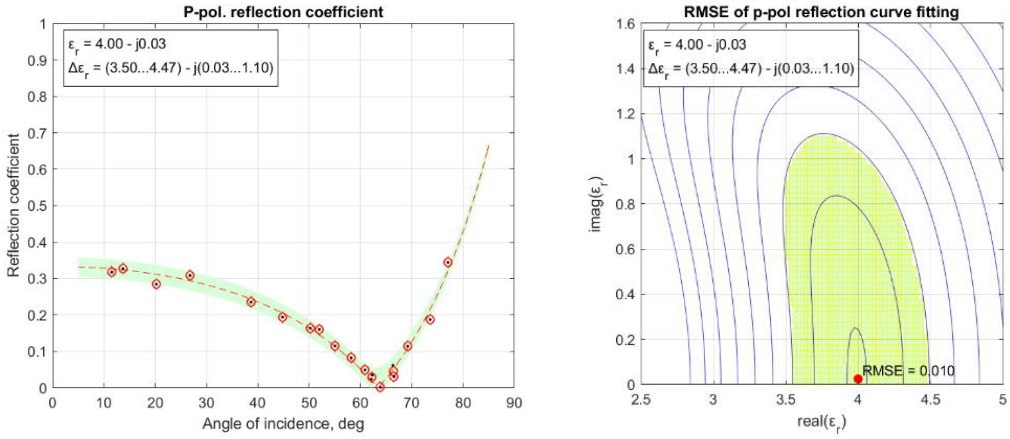

Figure 25: PR102 (white brick wall) at 1-18 GHz frequency range, RMSE<0.02.

Figures from Figure 26 through Figure 28 show the complex dielectric constant of the brick wall (perforated bricks, walled up side-ways, perforation visible) in PR102. Figures show the curve fitting and RMSE estimation results. Variation of the reflection coefficient is drawn using $\Delta\varepsilon_r$ from the range where RMSE<0.02.

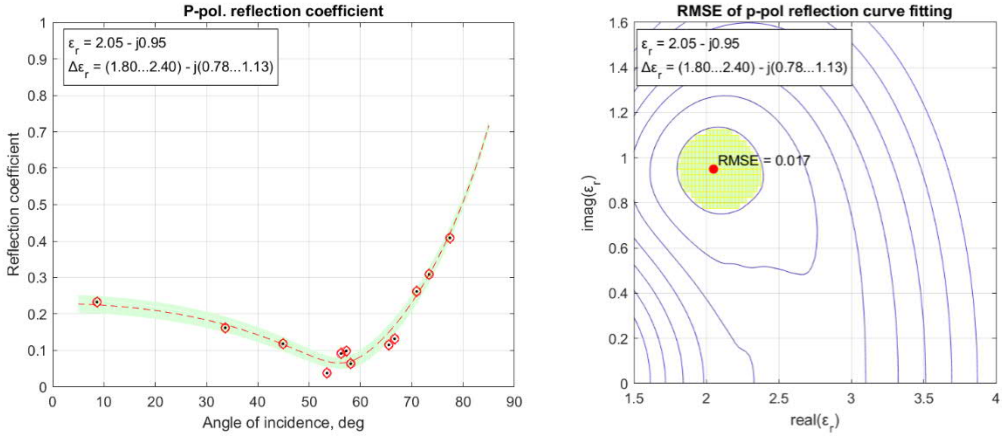

Figure 26: PR102 (red brick wall) at 1-9.5 GHz frequency range, RMSE<0.02.

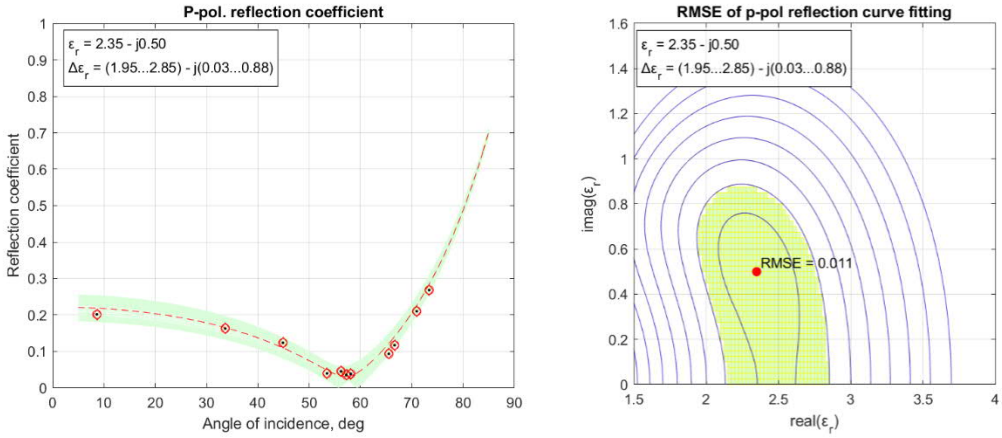

Figure 27: PR102 (red brick wall) at 9.5-18 GHz frequency range, RMSE<0.02.

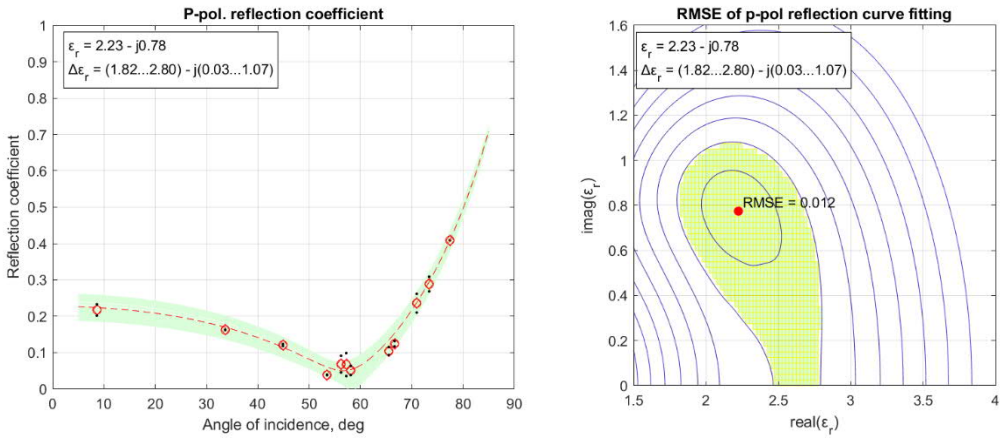

Figure 28: PR102 (red brick wall) at 1-18 GHz frequency range, RMSE<0.02.